The Faint Sky Variability Survey I:
Goals and Data reduction process

P.J. Groot[1,2,3], P.M. Vreeswijk[3], M.E. Huber[4,5], M.E. Everett[4], S.B. Howell[4],
G. Nelemans[3,6], J. van Paradijs[3,7], E.P.J. van den Heuvel[3], T. Augusteijn[8,9]
E. Kuulkers[10], R.G.M. Rutten[8], J. Storm[11]

[1] *Department of Astrophysics, University of Nijmegen, P.O. Box 9010, 6500 GL Nijmegen, The Netherlands*
[2] *Harvard-Smithsonian Center for Astrophysics, 60 Garden Street, Cambridge, 02138 MA, USA*
[3] *Astronomical Institute 'Anton Pannekoek'/ CHEAF, Kruislaan 403, 1098 SJ, Amsterdam, The Netherlands*
[4] *Astrophysics Group, Planetary Science Institute, 620 N. 6th Ave., Tucson, AZ, USA*
[5] *Department of Physics and Astronomy, University of Wyoming, PO Box 3905, Laramie, WY 82071, USA*
[6] *Institute of Astronomy, University of Cambridge, Madingley Road, CB3 0HA, Cambridge, UK*
[7] *Physics Department, University of Alabama in Huntsville, Huntsville, USA*
[8] *Isaac Newton Group of Telescopes, Apartado de Correos 321, 38700 Sta Cruz de La Palma, Canary Islands, Spain*
[9] *Nordic Optical Telescope, Apartado de Correos 474, 38700 S/C de La Palma, Canary Islands, Spain*
[10] *ESA-ESTEC, Science Operations & Data Systems Division, SCI-SDG, Keplerlaan 1, 2201 AZ Noordwijk, The Netherlands*
[11] *Astrophysikalisches Institut Potsdam, An der Sternwarte 16, D-14482, Potsdam, Germany*

13 July 2011

ABSTRACT

The Faint Sky Variability Survey is aimed at finding photometric and/or astrometric variable objects in the brightness range between $\sim16^{th}$ and $\sim24^{th}$ magnitude on timescales between tens of minutes and years with photometric precisions ranging from 3 millimagnitudes for the brightest to 0.2 magnitudes for the faintest objects. An area of ~23 square degrees, located at mid and high Galactic latitudes, has been covered using the Wide Field Camera on the 2.5m Isaac Newton Telescope on La Palma. Here we describe the main goals of the Faint Sky Variability Survey and the data reduction process.

1 INTRODUCTION

The advance of large format ($>$2k$\times$2k) CCDs with high quantum efficiency has opened up a new area in Galactic and extragalactic astrophysics: the systematic study of astrophysical objects fainter than 20th magnitude. The importance of this brightness regime is nicely illustrated by the current, fast development in the field of γ-ray bursts (GRBs; for a recent review see Van Paradijs, Kouveliotou and Wijers, 2000), where the localization of faint variable optical counterparts has led to a large increase in our understanding of GRBs.

In the following sections we will outline the main goals of the Faint Sky Variability Survey* (FSVS, Sect. 2), the INT Wide Field Camera (Sect. 3), the observing strategy (Sect. 4) and field selection (Sect. 5). After a short comparison with other, running surveys (Sect. 6), we will discuss data reduction (Sect. 7), final data products (Sect. 8) and availability of the data (Sect. 9).

2 GOALS OF THE FSVS

Understanding the variability of stars has often been crucial in the development of astrophysics, with applications ranging from the evolution of stars, to the structure of our Galaxy and the distance scale of the Universe. Current variability studies are mainly restricted to either bright regimes (brighter than 20th magnitude) or smaller areas (high-z supernovae and GRB searches). In the Galaxy, a deep variability study will not only reveal the characteristics of specific groups of stellar objects, but will also shed light on the outer parts of our Solar System, the direct Solar Neighbourhood, the structure of our Galaxy, and the extent of the Galactic halo. The FSVS has observed ~23 square degrees ($23^\square$) down to 24th magnitude. The main targets can be divided into two broad areas of interest: photometrically and astrometrically variable objects.

2.1 Photometrically variable objects

Among the various classes of variable stars our main targets are:

- *Close Binaries*:
Current detections of low-mass close-binary systems (Cat-

aclysmic Variables, Low-Mass X-Ray Binaries (LMXBs, including Soft X-Ray Transients, SXTs) and AM CVn stars) are strongly biased to small subsets of their populations. Of these systems the Cataclysmic Variables (CVs) form the main subgroup we expect to find. We refer to Warner (1995a) for an extensive review of CV properties, Van Paradijs & McClintock (1995) for optical observations of LMXBs and Warner (1995b) for AM CVn stars. Apart from novae, most CVs are either found as by-products of extragalactic studies like blue-excess, quasar surveys (e.g. the Palomar-Green survey: Green, Schmidt and Liebert, 1986; the Hamburg Quasar Survey: Engels et al., 1994; the Hamburg-ESO Quasar Survey: Wisotzki et al., 1996; and the Edingburgh-Cape Survey: Stobie et al., 1988), or by their outbursts in which the system suddenly brightens 3-10 magnitudes due to enhanced mass transfer through the accretion disk. However, theoretical calculations show that the majority of the CV population should have evolved down to mass-transfer rates that are lower than $\sim 10^{-11}$ $M_\odot$ yr^{-1} (see e.g. Kolb 1993; Howell, Rappaport and Politano, 1997; Howell, Nelson and Rappaport, 2001; however, see Patterson, 2001 for an alternative view). At these very low-mass transfer rates, CVs are expected to be faint (typically V>20), have no UV excess, show no (frequent) outbursts, and will therefore not show up in conventional searches. However, all CVs show intrinsic variability of the order of tenths of magnitudes or more. This variability is either caused by 'flickering' (mass-transfer instabilities), orbital modulations (hot spots or eclipses) or long-term mass-transfer fluctuations. Searching for faint variable stars is therefore a good way to define the characteristics of the majority of the CV population. Based on population synthesis models we expect to find 20 new CVs per square degree (Howell et al., 1997). The same search technique will also make the survey sensitive to other classes of close binaries, such as LMXBs, SXTs in quiescence and AM CVn stars.

• *RR Lyrae stars:*
Due to their standard candle properties and easy recognition by colour and variability, RR Lyrae stars can be used as excellent tracers of the structure of the Galactic halo. A few of these stars have been found at large galactocentric distances (Hawkins, 1984; Ciardullo et al., 1989), but number statistics are still poor. Finding more of these stars will help to constrain the total enveloped mass in the Galaxy at different radii. From the small number of known systems we derive a very uncertain estimate of 0.2 RR Lyrae stars per square degree that are beyond 30kpc.

• *Optical Transients to GRBs:*
The detection of optical counterparts to GRBs (e.g. Van Paradijs et al., 1997), and the subsequent classification of GRBs as cosmological (e.g. Metzger et al., 1997, Kulkarni et al., 1998) have shown that GRBs are among the most energetic phenomena known in the Universe. The high energies implied by observations of GRB afterglows (10^{53-54} erg in γ-rays if isotropy is assumed, Kulkarni et al., 1998; 1999), raises the question whether GRBs are emitting their energy isotropically or in the form of jets. In the latter case the energies involved will be much lower, depending on the amount of beaming. Even if the γ-rays are beamed the optical afterglow is expected to radiate more isotropically, and thus one expects to observe faint afterglows without an accompanying burst in γ-rays. The detection rate of such transient events will constrain the beaming angle. The expected detection rate depends very much on the chosen geometry of the GRBs and varies for the FSVS database between several dozens and ≪1. A discussion and analysis of our results is presented in Vreeswijk (2002).

2.2 Astrometrically variable objects

The observing schedule that we have adopted for the FSVS (see Sect. 4) also allows for the detection of astrometrically variable objects. Our interests fall into two main categories:

• *Kuiper Belt Objects:*
Kuiper Belt Objects (KBOs) are icy bodies revolving around the Sun in orbits that lie outside the orbit of Neptune (which has led to the alternative name of Trans Neptunian Objects; TNOs). Since their discovery in 1993 (Jewitt and Luu, 1993), more than 100 of these objects have been found. Studying their properties will give important insight into the formation of the Solar system and planetary systems in general. One question that is particularly well suited to be answered is the inclination distribution of KBOs. Most KBOs have been found within 5° from the ecliptic, but this may constitute an observational bias, since most searches have been (and are) performed close to the ecliptic. Since the FSVS is mostly pointing away from the ecliptic, we will be able to set limits on the inclination distribution of KBO's. KBO's are found from intra-night astrometric variability. One KBO is found so far in a preliminary search of the FSVS database (K01QW2X; Gladman et al., 2001).

• *Solar Neighbourhood Objects:*
The yearly re-observations allow for the detection of high proper-motion objects in the Solar neighbourhood. These will be extremely important to constrain the low-mass end of the IMF in the solar neighbourhood, to estimate the relative contribution of the disk and halo population of stars in the solar neighbourhood and trace the star formation history of the Galactic halo by finding old, high proper motion, white dwarfs.

3 THE INT WIDE FIELD CAMERA

The Wide Field Camera[†] (WFC) is mounted at the prime focus of the 2.5m Isaac Newton Telescope (INT) at the Observatorio del Roque de Los Muchachos on the island of La Palma. The WFC consists of 4 EEV42 CCDs, each containing 2048×4100 pixels. They are fitted in an L-shaped pattern, which makes the Camera 6k×6k, minus a 2k×2k corner (see Figure 1). The CCDs consist of 13.5μ pixels (0.″33 per pixel on the sky), which gives a sky coverage per CCD of 22.′8×11.′4. A total of 0.□29 is covered by the combined four CCDs. With a typical seeing of 1.″0-1.″3 on the INT, point objects are well-sampled, which allows for accurate photometry. The Camera is equiped with Harris and Sloan filters, of which we use the Harris B, V and I filter. Zeropoints, defined as the magnitude that gives 1 detected e$^-$/s, in these filters are 25.6 in B and V and 25.0 in I.

[†] see: http://www.ast.cam.ac.uk/∼wfcsur/index.php for an extensive description of the WFC
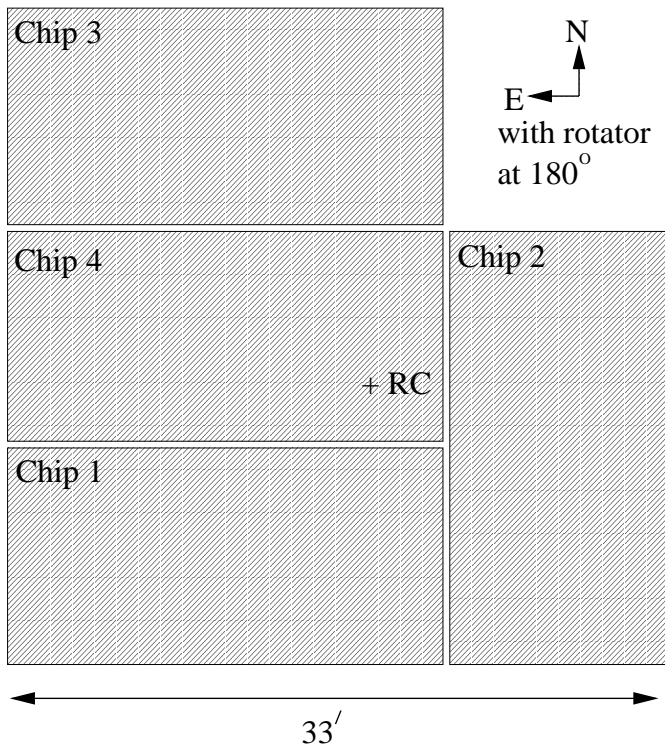
Figure 1. Graphical lay-out of the WFC 4 EEV 4k×2k CCDs. In the orientation used by the FSVS, North is up and East is to the left. The WFC rotates around its Rotator Center (RC).

Table 1. Field centers and period of observations of the FSVS fields. All coordinates are in J2000 units.

Field No.	RA	Dec	l^{II}	b^{II}	Period
1-6	23^h44^m	$+27°15'$	105	−33	Nov 98
7-12	02^h32^m	$+15°00'$	156	−40	Nov 98
13-18	07^h52^m	$+20°40'$	200	+22	Nov 98
19-22	12^h53^m	$+27°01'$	220-21	+90	May 99
23-26	12^h51^m	$+26°20'$	268-360	+89	May 99
27-30	16^h25^m	$+26°33'$	45	+43	May 99
31-34	17^h20^m	$+27°00'$	49	+31	May 99/00
35-40	03^h02^m	$+18°38'$	161	−33	Jan 00/01
41-46,59	07^h15^m	$+21°00'$	196	+15	Jan 00/01
47-52,60	10^h00^m	$+21°30'$	211	+50	Jan 00/01
52-56	16^h23^m	$+27°03'$	45	+42	May 00
57-58	16^h32^m	$+21°16'$	39	+39	May 00
61-62	10^h37^m	$+04°00'$	242	+50	Jan 01
63-66	17^h25^m	$+27°30'$	50	+30	Jul 01
68-71	22^h02^m	$+27°30'$	83	−21	Jul 01
72-75	18^h32^m	$+36°00'$	64	+19	Aug 01
76-79	23^h47^m	$+28°10'$	106	−32	Aug 01

5 FIELD SELECTION

The field selection was governed by the following four criteria (in order of importance) to ensure maximum quality of the data:

• Fields are located at Galactic latitudes $b^{II} > 20°$: to probe the Galactic halo as well as the Galactic disk to considerable depths we target most of our fields at mid-Galactic latitudes (see Table 1). This also prevents problems with field crowding and interstellar extinction that will be present at lower Galactic latitudes.

• Fields are observed within a zenith distance, $z < 30°$: this criterion has been set to limit the effect of differential extinction coefficients on the accuracy of the photometry.

• If possible we select our fields at the ecliptic, to increase the chances of finding KBOs. However, as explained in Sect. 2.2 even if we are not able to point at the ecliptic, our results may help to constrain the inclination distribution of KBOs.

• Bright stars are avoided: stars brighter than ∼10th magnitude will cause large charge overflows and diffraction patterns that limit the area on a CCD that can be used for accurate photometry, depending on the placement and brightness of the star. To prevent this from happening the fields are selected to be as devoid as possible of bright stars. We checked for the presence of bright stars using the Digital Sky Survey in the selection of the fields.

It is clear that not all four criteria can always be met. For the Northern Hemisphere all four criteria can only be met in late November-early December. Table 1 shows the center points of the FSVS fields, together with the Galactic coordinates and period of first observations.

6 COMPARISON WITH OTHER SURVEYS

The FSVS is unique in its search for variability on short timescales (tens of minutes to days), depth and precision of its differential photometry, although having a rather moderate sky-coverage. The Sloan Digital Sky Survey (SDSS; York et al., 2000) covers a much larger area of the sky (10 000 $^\square$), but at brighter magnitudes ($14 < g' < 22.5$), and provides

4 OBSERVING STRATEGY

The typical timescales of variability covered by the objects listed above vary from hours (CVs, KBOs, RR Lyrae stars) to days (optical transients to GRBs) to years (high proper motion stars). To cover all possible timescales of variation we have devised an observing strategy that optimises both the coverage per field as well as the total sky coverage. The variability search is done with 10 min. V-band observations. This is a compromise between the expected colours of our targets and the sensitivity of the WFC which peaks between 4000Å and 6000Å or the photometric variability we find that at least 15-20 pointings are needed to firmly state that an object is variable and also get an indication of the timescale of its variability (or ideally its period). For the first two runs of the FSVS this number was limited to ∼10, but has been raised to 15-20 in subsequent runs.

The FSVS has been observing in one-week time slots, separated by roughly half year intervals. Observations of one field are mainly obtained within the one week observing run, with single observations in the yearly returns. In the observing sequences we have tried to avoid a regular spacing of the observations since this will introduce strong aliases in any period search. On photometric nights (which were always present in each of the runs) the fields were observed in B (10 min) and I (15 min) together with Landolt (1992) fields. These observations were taken centered on each of the four chips to obtain a sufficient number of photometric standards per chip (see Sect. 7.9). Using this observing strategy an average of $4^\square$ per one-week run was observed. Single V-band re-observations of each field are being obtained on a yearly basis.
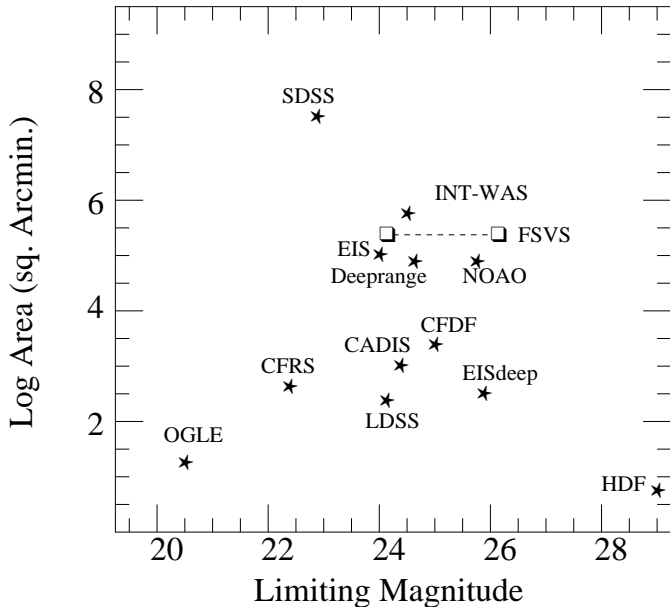
Figure 2. A comparison in area and depth between major current surveys and the FSVS. Adapted from the NOAO Deep Survey Web-pages (see http://www.noao.edu/noao/noaodeep/; SDSS=Sloan Digital Sky Survey, York, et al., 2000; EIS(deep) = ESO Imaging Survey (Deep), Nonino et al., 1999; Deeprange = Postman et al. 1998; INT-WAS: INT Wide Angle Survey: McMahon et al., 2001; HDF= Hubble Deep Field, Williams et al., 1996; NOAO= NOAO Survey, Jannuzi and Dey, 1999; CFRS = Canada France Redshift Survey, Lilly et al., 1995; CADIS = Calar Alto Deep Imaging Survey, Hippelein et al., 1998; CFDF = Canadian French Deep Fields; Brodwin et al., 1999; LDSS=Glazebrook et al., 1995; OGLE = Optical Gravitational Lensing Experiment, Udalski et al., 1992). Note that most of these surveys have no or very limited variability information. The range in depth for the FSVS corresponds to using each individual image (as in the variability study) or the sum images.

almost no variability information. The microlensing studies (e.g. MACHO, Alcock et al., 1997; EROS, Beaulieu et al., 1995; OGLE, Udalski et al., 1992) do obtain variability information, but are targeted at different stellar populations (the Galactic Bulge, the LMC, or M31) and have a limit of V~21 with a photometric precision of 0.5 mag at the faint end, caused by limited S/N and crowding in their necessarily high density star fields. High z supernovae searches reach as deep as the FSVS, but have a lower time-resolution and smaller area. In Figure 2 we show schematically how the FSVS compares with other deep ongoing surveys.

7   REDUCTION AND ANALYSIS METHODS

To obtain variability information on all the objects detected in our observations we use the technique of differential aperture and psf photometry. We have written a pipe-line reduction package, consisting of IRAF tasks, Fortran programs and at its core the SExtractor program by Bertin and Arnouts (1996). Every object in every observation is analysed and the results are stored in a master-table that lists the essential information (described below in detail) for each object. Below we outline the data flow through our

pipe-line reduction, starting with the raw data as it comes from the telescope.

7.1   Bias subtraction

The mean of the counts in the overscan region of each observation is used to subtract the overall bias level. After this the 2-D bias pattern, determined from bias observations taken at the start of the night, is subtracted.

7.2   Linearization of the data

A non-linearity in the read-out electronics causes all data taken with the INT WFC to be non-linear up to a level of ~5%. The magnitude of this non-linearity as a function of exposure level is determined by the Cambridge WFS group[†] and is posted in tabular and analytic form. These corrections are applied after bias-subtraction.

7.3   Flatfielding

From twilight skyflats taken during a complete observing run a master flatfield is made, which is used for all the observations taken in that band during the observing run. For the I-band observations, which suffer from fringing at the 3.5% level, we have made fringe maps from the night time observations, which allows the fringe pattern to be removed down to the 0.6% continuum sky level (see Fig. 3).

7.4   Source detection

The bias-subtracted, linearized and flat-fielded data are fed to the SExtractor program. This program detects sources and measures their instrumental magnitude in a number of different ways, as set by the user. Source detection is done by requiring that three neighbouring pixels are more than two sigma above the sky-background. Visual inspection shows that this threshold value is capable of detecting virtually all objects that can be identified by eye. Some contamination from extended cosmic rays is present, but these are effectively removed in the subsequent steps. Apart from finding the sources and determining their instrumental magnitudes, for each source the SExtractor program determines other characteristic parameters such as the position, size, extent, ellipticity and orientation angle. Due to vignetting a corner of CCD3 (the NE corner in Fig. 1) has very low count rates. We discard any object detected in a square box 200 pixels wide from this corner of CCD3. Spatial offsets between observations of the same fields in different visits are small (typically $<20''$) so no check is made for detections on different CCDs.

7.5   Instrumental magnitudes

For each object instrumental magnitudes are extracted in four different ways: fixed aperture photometry, seeing matched aperture photometry, variable psf fitting photometry and isophotal magnitudes. The isophotal magnitudes

[†] see: previous footnote for URL and details

and fixed 12 pixel radius aperture photometry have been included as a check on the others and for extragalactic work in case of the isophotal magnitudes. The seeing matched aperture photometry uses an aperture that scales with the seeing of the observations. This seeing is determined using bright unsaturated stars in the inner 1k × 1k region of each chip. The size of the aperture for the observation is set to twice the FWHM of the seeing estimate. This relatively large aperture works well for bright stars, but the S/N deteriorates for faint objects due to the dominant sky background. In Fig. 4 we show the variation of the error for an aperture of twice the seeing FWHM and for an aperture of one time the FWHM. This clearly shows that for bright stars they work equally well and for faint stars small apertures work better. However, in Sect. 7.8 we will show that the aperture photometry is not ideal for variability studies.

The error on the instrumental magnitudes is determined only by Poisson-statistics, including the source and background brightness, read-out noise of the chip and the gain.

In the variable psf fitting the point-spread-function of the objects, and its variation, over the chip is determined from a set of 25 isolated stars, spread equally in position over the chip. Using this variable psf the instrumental magnitude of each object is determined with the use of the IRAF DAOPHOT package, in which the photometric accuracy is adjusted from 1 mmag to 0.1 mmag to be able to obtain the photometric precision needed for the brightest stars. The error in the instrumental magnitude is now a combination of the Poisson statistics (as in the aperture photometry) as well as a factor from the fitting procedure. This causes the psf errors on the brightest objects to be higher than in the aperture photometry (see Fig. 4), but for the faint sources it is as good as that of the 1×FWHM aperture photometry.

Although from just Fig. 4 it would seem that the aperture photometry is doing much better than the psf photometry at the brighter end, the variability study (as discussed in Sect. 7.8) shows this not to be the case. The Poisson errors on the aperture photometry are not a good representation of the actual error on the measurement. Other sources of errors besides counting statistics such as low-level gain and read-out noise variations, flatfield errors and a variable psf become dominant at bright magnitudes. This shows up as a flattening of the error distribution. In Sect. 7.8 we will show that the small aperture photometry errors introduce apparent variability for the brightest stars and therfore aperture photometry is therefore not the most suitable for the FSVS.

7.6 Field matching

Different observations of the same field are automatically matched using the OFFSET program, supplied with the DOPHOT package (Schechter, Mateo and Saha; 1993), using the 100 brightest, non-saturated stars, that are not located near the edges of the CCDs. Matching is done by triangle pattern recognition in the two images. This matching allows for linear scaling, rotation and translation of the different images. Output is given as the elements of a rotation-
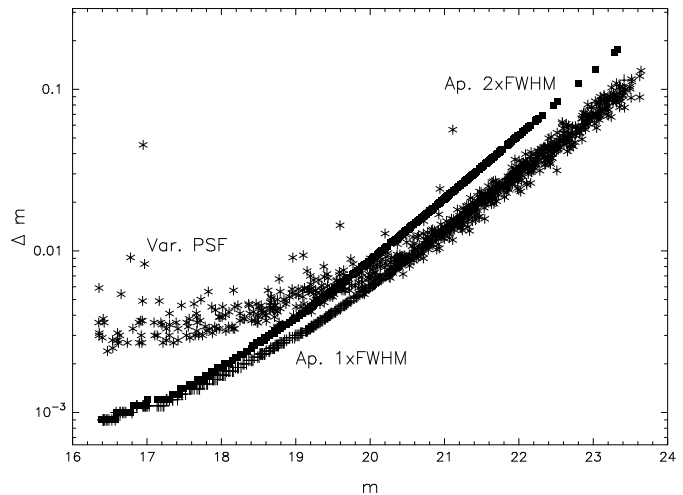

Figure 4. Instrumental photometric errors per magnitude for seeing matched aperture photometry with 1×FWHM (+-signs), 2×seeing FWHM (filled squares) and variable psf fitting (stars).

translation matrix. All image source catalogues are transformed to that of a reference image (the one with the best seeing). Individual objects are matched if in the new image an object is found within 1 FWHM of the position of the object in the reference image. This same criterion is used to match stars between different filters.

7.7 Local reference star selection

In order to obtain differential magnitudes, an ensemble of local reference stars has to be selected. The average (ensemble) magnitude of these stars is used as a baseline to compute all instrumental magnitudes. In the selection of this ensemble it is important to use the brightest, non-variable, stars that are not saturated. Using the brightest stars is essential because the error on the differential magnitude of any object consists of the error that is obtained from counting statistics for that object, and the error on the average of the reference stars (see e.g. Howell, Mitchell and Warnock, 1988). The uncertainty in the mean magnitude of the ensemble must be made significantly smaller than the uncertainty imposed by counting statistics on the magnitude of any star of interest. If this is not the case, it will cause small-amplitude variability, that should have been detected on the basis of counting statistics, to become undetectable. Per CCD, an ensemble of ten local standards is selected by requiring that their variation with respect to the average is less than 5 millimagnitudes. If this requirement is set more stringently not enough standards are found. In the Galactic North Pole observations of May 1999 the selection criterion had to be relaxed to 10 millimagnitudes in order to find a suitable number of stars. This is, of course, due to the limited number of stars in the NGP direction. As explained above, this selection criterion naturally sets the minimum amplitude ($=$ scatter$/\sqrt{N_{\text{reference stars}}}$) of variation that can be found. We have not taken a colour

difference between the ensemble and targets stars into account. However, this small effect will only be important for the brightest stars, which, on average, will also have similar colours to the ensemble stars.

7.8 Differential magnitudes and variability

For every object the differential magnitude is calculated against the ensemble average. The error of the instrumental magnitude is propagated to the differential magnitude, adding quadratically to the error on the ensemble average. The error on the ensemble average is determined from the scatter of the ensemble stars at that epoch around their average over all epochs. The differential magnitude is calculated for all four instrumental magnitudes as described in Sect. 7.5 for all observations of this field. In Fig. 5 we show the variation around their average magnitude for all objects in a representative field of the FSVS, both for seeing matched aperture photometry as well as for the variable PSF fitting. The rise towards fainter magnitudes is a consequence of the larger instrumental magnitudes errors due to lower count rates. For the brightest sources a differential magnitude variation of < 5 mmag, which is at the level of extrasolar planet transits, is easily obtained.

Variability is determined by calculating the reduced χ^2 value of the light curve with respect to its average value. As expected this is a constant as a function of magnitude (Fig. 6). In Fig. 6 we show the χ^2 distribution for the $1\times$FWHM aperture (bottom), and $2\times$FWHM aperture photometry (middle) and the variable psf fitting (top). The dashed line in Fig. 6 shows the 5-σ variability level above which we denote our stars to be variable. From this we see that an aperture of $1\times$FWHM is too small for the bright stars and introduces spurious variability. The $2\times$FWHM also suffers from spurious variability, although that is not immediately clear from Fig. 6.

Despite the accurate photometry on a single epoch, the $2\times$FWHM aperture photometry suffers from the introduction of systematic variability into the light curves due to the basic assumption of aperture photometry that the psf is the same for all objects in the field. The chips of the WFC are slightly tilted with respect to the focal plane of the camera, which introduces a variation in the psf of $\sim 20\%$ over the field of a single chip. When analysed with aperture photometry this introduces spurious variability both at the bright end as well as at the fainter end of the magnitude range. At the bright end the variation is caused by the change of the psf due to tilt of the CCDs. At the fainter end the change is caused by barely resolved binaries and compact galaxies. Not including this source of error in the aperture photometry at the bright end causes the high number of spurious variables. In the PSF fitting these errors are taken into account (as can be seen from the higher level of single-epoch errors in Fig. 4), and the spurious variability is removed (see Fig. 5 and 6). The fact that the average χ^2-value for the psf-fitting lies around 1 for the non-variable stars at all magnitudes shows that the psf errors are an accurate reflection of the true uncertainties on the individual photometric measurements.
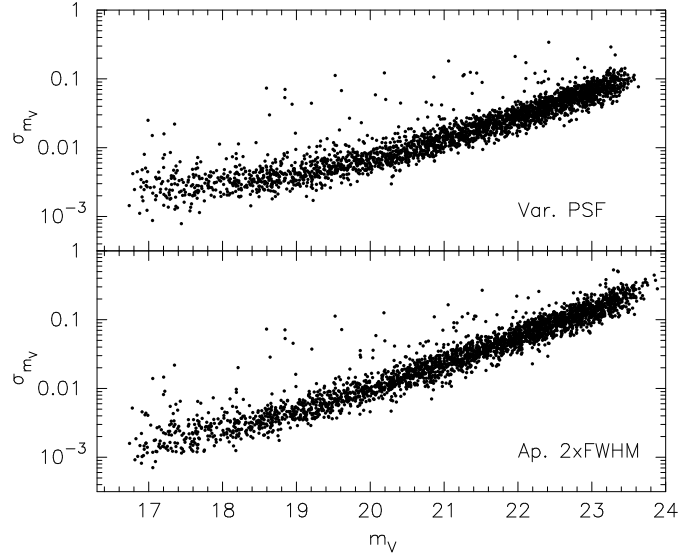

Figure 5. The standard deviation on the light curves of point sources (stellarity >0.8) in the same field as shown in Fig. 4. *Top* for Variable PSF fitting and *bottom* for $2\times$seeing FWHM aperture photometry.
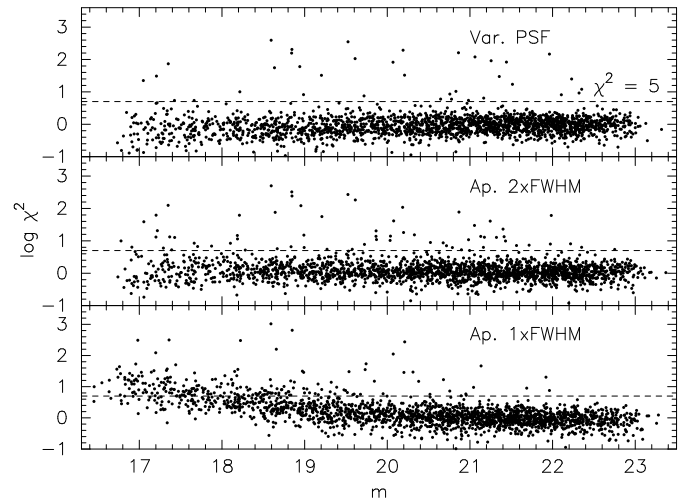

Figure 6. Variability distributions for the same field as shown in Figs. 4 and 5. *Bottom:* seeing matched aperture photometry with aperture size equal to $1\times$ seeing FWHM. *Middle:* same as bottom but with aperture size $2\times$FWHM. *Top:* variable psf fitting.

7.9 Astrometric and photometric calibration

Using the USNO A2.0 catalogue an astrometric solution is obtained for each CCD and each field separately. On average, we use 20-30 USNO A2.0 stars, which is sufficient to obtain a cubic solution that is accurate to $0.''2$-$0.''4$ in right ascension and declination, depending on the position of a field on the sky.

During each of our runs, we have had photometric nights, during which all fields and several Selected Areas of Landolt (1992) were observed. After having found the astrometric solution for the standard stars, we can measure the standard stars automatically. We use the SExtractor aperture photometry option, with an aperture radius of twice

the image FWHM. For each CCD the measured B, V and I standard star magnitudes are fitted to a model that includes a zero-point offset, an airmass term and a colour term. When sufficient standards are observed at different airmasses, we fit for the airmass term. If not, we hold it constant at the following values: 0.25, 0.15 and 0.07 for the filters B, V and I, respectively[†]. The colour term is only included if it improves the fit significantly. These solutions are applied to all objects listed in the catalogue through the ensemble reference stars that are selected for each CCD of each field (see Sect. 7.7). From the scatter in the solutions, we estimate the error in the absolute calibration to be 0.05 for the B and V filters, and 0.1 for the I band.

7.10 Limiting magnitudes

Based on the amount of flux in the ten reference stars (see Sect. 7.7), the level of the background sky, the photometry aperture size and the background aperture size, we calculate the a 3-, 5-, and 7-sigma limiting magnitude object for each CCD, field and observation. In this calculation we neglect the read-out noise since our observations are long and have background levels whose noise is much higher than the read-out noise. On average the 5-sigma limiting magnitudes range between 22.5-24.5 for the B and V-band images (depending on seeing and cloud cover) and between 21.5 and 23.5 for the I-band observations.

7.11 Star - Galaxy separation

The star-galaxy separation used in the FSVS is based on the 'stellarity' parameter, as returned from the SExtractor routines (Bertin and Arnouts, 1996). This parameter has a value between 0 (highly extended) and 1 (point source). In the FSVS the stellarity value of an object is taken as the value in the combined V-band images. Due to the increased S/N in this image, the star-galaxy separation can be done reliably almost 1 magnitude deeper than from any individual image. As can be seen in Fig. 7 this separation of object types works very well to classify point-sources (with a value >0.8) down to V~23.5-24. Fainter stars tend to have slightly lower stellarity values (they turn down between V=23 and V=24) but can still be well separated from the galaxies, although some stars at the faint end of the distribution may be mis-classified as extended.

7.12 Astrometric variables

The proper motion analysis is currently not included in the standard pipe-line reduction but is handled separately using either the reduced images (in the case of Kuiper Belt Objects) or the SExtractor output and astrometric solution as provided by the pipeline (in the case of the high proper motion stars). Details on both analyses will be given in subsequent papers. Our first results indicate that proper motions will be measurable down to 10 mas yr^{-1} with a 2-year baseline.
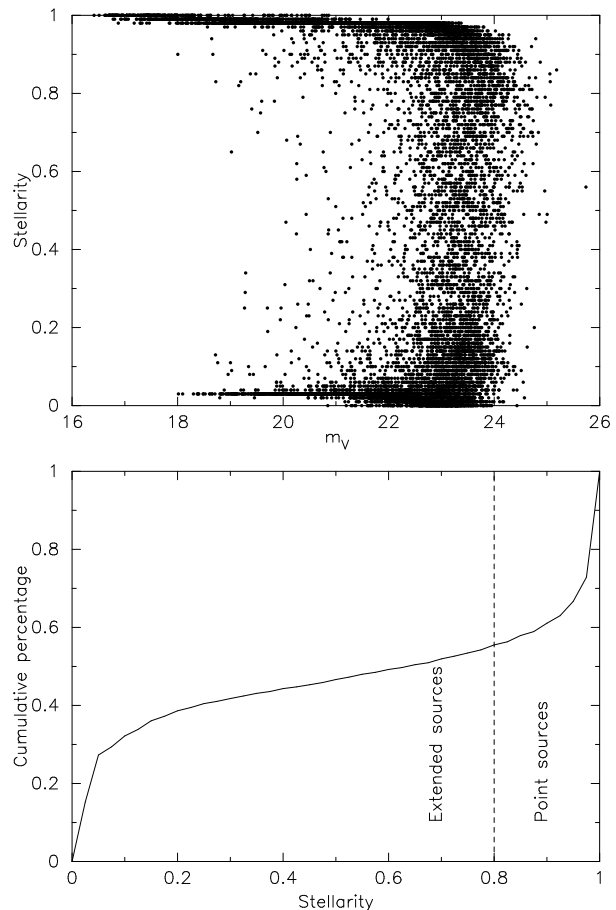
[†] see first WFC footnote

Figure 7. *Top:* The stellarity versus magnitude for one of our fields. A stellarity of zero indicates a highly extended source, and a stellarity of one is a point-source. Detections at V>25 are noise spikes. *Bottom:* The cumulative distribution of sources over stellarity values down to V=24. Using a point source cut-off of 0.8, we have ~45% of objects as point sources.

8 FINAL PRODUCTS

The pipeline discussed above returns two sets of output files:
• The reduced images
• The data tables with the photometric and astrometric information.
The data tables are made per field, per CCD and are made for four different magnitudes: the psf magnitude, the fixed aperture magnitude, the isophotal magnitude and seeing matched aperture magnitude.

The header of the table contains all relevant information on the exposures: run numbers of the original frames, the HJDs of the observations, the filter, the airmass, the average FWHM of the point sources in the observation (the 'seeing'), the six element rotation-translation matrix to the reference image and the 3-, 5-, and 7-σ limiting magnitude of the image. The data tables contain, for each detected object: name, position and colour, followed by the magnitude, error on the magnitude, fwhm, stellarity and the error flag as returned from the SExtractor program for each observation.

If an object is only detected in a subset of all the observations, it is added to the final catalogue, and dummy values

(any decimal combination of 9's, e.g. 99.999 , 9.99 etc.) are introduced when it was not detected.

The object names are given in standard IAU format as FSVSJhhmmss.ss+ddmmss.s, all in J2000 coordinates. Each object is also given an 'internal' name whose format is F_XX_Y_ZZZZZ, with XX the field number, Y the CCD number (1-4) and ZZZZZ a five digit detection number. The position of each object is given both in RA and DEC as well as in x,y-coordinates in the reference frame of the specific field.

9   AVAILABILITY OF THE DATA

All raw images are available upon request from the ING-WFS archive in Cambridge after the one year propietary right. For UK and NL astronomers the data is immediately available. All ASCII data-tables, containing the reduced information described above, are retrievable from the FSVS website.

10   CONCLUSIONS

The FSVS offers a unique possibility of studying the behaviour of variable objects in the magnitude range of $16 < V < 24$ with photometric precisions ranging from 3 millimag (at $V=16$) to 0.2 mag (at $V \simeq 24$).

Besides the study of variable objects, the FSVS offers a large dataset that can serve as the basis for many research topics (e.g. YSO's, gravitational lenses, galaxy counts, quasar searches). The FSVS-collaboration encourages the use of the data set for all purposes.

REFERENCES

Alcock, C., et al., 1997, ApJ 486, 697
Beaulieu, J.P., et al., 1995, A&A 303, 137
Bertin, E. and Arnouts, S., 1996, A&AS 117, 393
Brodwin, M., Lilly, S. and Crampton, D., 1999, in *Photometric Redshifts and the Detection of High Redshift Galaxies*, ed., Weymann et al., ASP Conf. Ser. 191, p. 105
Ciardullo, R., Jacoby, G.H., Bond, H.E., 1989, AJ 98, 1648
Engels, D., Cordis, L., Köhler, T., 1994, in *IAU Symp. 161*, eds. H.T. MacGillivray et al. (Kluwer, Dordrecht), p. 317
Gladman, B.; Kavelaars, J.; Wasserman, L. H., et al., 2001, MPEC 2001-V57
Glazebrook, K., Ellis, R., Colless, M., et al., 1995, MNRAS 273, 157
Green, R.F., Schmidt, M. and Liebert, J., 1986, ApJS, 61, 305
Hawkins, M.R.S., 1984, MNRAS 206, 433
Hippelein, H., Beckwith, S., Fockenbrock, K., et al., 1998, in *New Horizons from Multi-Wavelength Sky Surveys*, ed. McLean, Golombek, Hayes, and Payne, IAUS 179, p 292
Howell, S.B., Mitchell, K.J and Warnock, A., 1988, AJ 95, 247
Howell, S.B., Rappaport, S. and Politano, M.R., 1997, MNRAS 287, 929
Howell, S.B., Nelson, L. and Rappaport, S., 2001, ApJ 550, 897
Jannuzi, B.T. and Dey, A., 1999, in *Proc. Photometric redshifts and the Detection of High Redshift Galaxies*, ed. Weymann et al., ASP Conf. Ser. 191, p. 111
Jewitt, D. and Luu, J., 1993, Nature 362, 730
Kolb, U., 1993, A&A 271, 149
Kulkarni, S.R., et al., 1998, Nature 393, 35
Kulkarni, S.R., et al., 1999, Nature 398, 389
Landolt, A.U., 1992, AJ 104, 340
Lilly, S.J., Le Fevre, O., Crampton, D., Hammer, F. and Tresse, L., 1995, ApJ 455, 50
McMahon, R., et al., 2001, New Astr. Rev. 45, 97
Metzger, M.,R., et al., 1997, Nature 387, 878
Nonino, M., et al., 1999, A&AS 137, 51
Patterson, J., 2001, PASP 113, 736
Postman, M., Lauer, T.R., Szapudi, I., Oegerle, W., 1998, ApJ 506, 33
Schechter, P.L., Mateo, M. and Saha, A., 1993, PASP 105,1342
Stobie, R.S., Morgan, D.H., Bhathia, R.K., Kilkenny, D. and O'Donoghue, D., 1988, in *The Second Conference on Faint Blue Stars*, IAU Colloq. 95, eds. D. Philip et al., David Press, Schenectady, NY, p. 43
Udalski, A., et al., 1992, Acta Astronomica 42, 253
Van Paradijs, J., Groot, P.J., Galama, T.J et al., 1997, Nature 386, 686
Van Paradijs, J., Kouveliotou, Ch. and Wijers, R.A.M.J., 2000, ARA&A 38, 379
Vreeswijk, P.M., 2002, PhD Thesis, University of Amsterdam
Warner, B., 1995a, *Cataclysmic Variables*, Cambridge Astrophysics Series 28, CUP, Cambridge, UK.
Warner, B., 1995b, Ap&SS 225, 249
Williams, R., et al., 1996, AJ 112, 1335
Wisotzki, L., Köhler, T., Groote, D and Reimers, D., 1996, A&AS 115, 227
York, D.G., et al., 2000, AJ 120, 1579

This figure "after.jpg" is available in "jpg" format from:

http://arxiv.org/ps/astro-ph/0210416v1

This figure "before.jpg" is available in "jpg" format from:

http://arxiv.org/ps/astro-ph/0210416v1

This figure "fringemap.jpg" is available in "jpg" format from:

http://arxiv.org/ps/astro-ph/0210416v1